Nanoscale

Accepted Manuscript

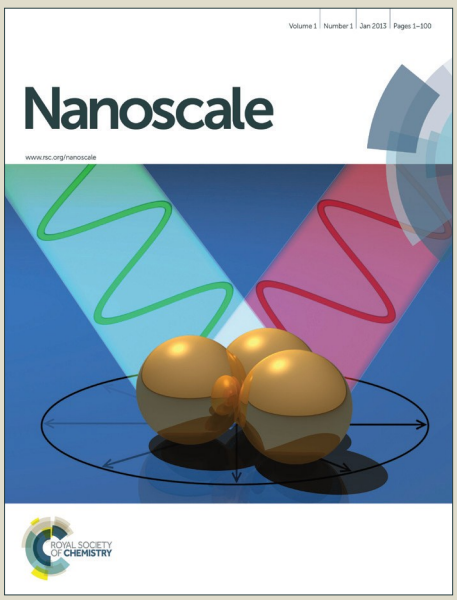

ROYAL SOCIETY OF CHEMISTRY

www.rsc.org/nanoscale

Nanoscale

ARTICLE

Effect of intra-membrane C_{60} fullerenes on modulus of elasticity and mechanical resistance of gel and fluid lipid bilayers

Cite this: DOI: 10.1039/xoxxooooox

Received ooth April 2015,
Accepted ooth April 2015

DOI: 10.1039/xoxxooooox

www.rsc.org/

[a,b]Jihan Zhou, [b]Dehai Liang and [a]Sonia Contera†

Penetration and partition of C_{60} to the lipid bilayer core are relevant both to C_{60} toxicity and useful to realise C_{60} biomedical potential. A key aspect is the effect of C_{60} on bilayer mechanical properties. Here, we present an experimental study on the mechanical effect of the incorporation of C_{60} in the hydrophobic core of fluid and gel phase zwitterionic phosphatidylcholine (PC) lipid bilayers. We demonstrate its incorporation inside the hydrophobic lipid core and the effect on the packing of the lipids and vesicle size using a combination infrared (IR) spectroscopy, atomic force microscopy (AFM) and laser light scattering. Using AFM force spectroscopy we measure the Young's modulus of elasticity (***E***) of 1,2-dipalmitoyl-sn-glycero-3-phosphocholine (DPPC), 1,2-dimyristoyl-sn-glycero-3-phosphocholine (DMPC) and 1,2-distearoyl-sn-glycero-3-phosphocholine (DSPC) in the absence (presence) of intra-membranous C_{60} at 24.5 °C. ***E*** of fluid phase supported bilayers is not altered by C_{60}, but ***E*** increases with incorporation of C_{60} in gel phase bilayers. The increase is higher for longer hydrocarbon chains: 1.6 times for DPPC and twice for DSPC. However the mechanical resistance of gel phase bilayers of curved bilayer structures decreases with the incorporation of C_{60}. Our combined results indicate that C_{60} causes a decrease in gel phase lipid mobility, *i.e.* an increase in membrane viscosity.

1. Introduction

In recent years there has been a resurgence of interest in the study of C_{60} fullerenes and their interactions with biological systems, and in particular with lipid membranes. C_{60}, unique carbon cage structure of 1 nm in diameter, its unique reproducibility in size and structure - still a rare characteristic in engineered nanoparticles- and an immense scope for derivatisation make them very attractive from both the technological[1] and biomedical[2, 3] points of view. Like many other nanoparticles that are used in biological environments C_{60} presents the apparently paradoxical property of being at the same time bio-medically attractive and potentially toxic[4, 5]. C_{60} has shown anti-HIV activity[6] and antimicrobial action[7] and has been used as magnetic resonance imaging agent[8]. C_{60} aggregates have been proposed as an anticancer-prodrug for chemo and photodynamic therapies[9]. C_{60} can inactivate intracellular free radicals, giving them unusual power to stop free radical injury and to halt the progression of diseases caused by oxidative stress such as Parkinson's[10], Alzheimer's[11], multiple sclerosis[12], sun skin damage and aging[13].

C_{60} interacts very strongly with lipid membranes. The interaction between C_{60} and lipids has been the object of intensive study for several reasons: (i) Lipids can be used for solubilisation of C_{60} by incorporation inside non-toxic liposomes[14, 15]. (ii) Liposomes are commonly used in drug delivery systems[16] and they could be used as a vehicle for delivering C_{60} with therapeutic or diagnostic applications. (iii) The interaction of C_{60} with lipid membranes is key to their potential toxicity.

Both experiments and simulations[17, 18] confirm that fullerenes partition to the membrane interior[15, 19]. The effects of C_{60} on bilayer dynamical and mechanical properties are important for toxicity and drug delivery[20, 21]. Rigidity is one of the key physical factors in improving the drug delivery efficiency of carrier particles[22], and it is starting to be exploited in mechano-sensitive drug-delivery systems[23, 24]. It affects their particulate stability and drug release profile as well as their blood circulation time. In this context incorporation of C_{60} might be an interesting way of achieving two goals: C_{60} can be used both as a drug and to modulate the mechanics of the liposome.

Mechanical effects of C_{60} on model system lipid bilayers have been recently studied by Wong-Ekkabut *et al.*[21] using computer simulations. They predicted a 40% decrease of the diffusion coefficient of lipids, *i.e.* increase in membrane viscosity. Furthermore a significant decrease in mechanical resistance of the membrane was predicted. Despite the significant changes in membrane properties upon the addition of C_{60}, the authors concluded that fullerenes could hardly cause any structural damage to the membrane, since no bilayer rupture, micellisation or persistent pore formation could be predicted in the simulations. Currently there are no experiments available, to the best of our knowledge, to confirm these simulations.

Here, we present an experimental study of the mechanical properties of fluid and gel phase zwitterionic lipid bilayers that contain C_{60} in their hydrophobic core. We use the mixed film method to produce liposomes containing C_{60}, IR spectroscopy to confirm their incorporation in the bilayer and laser light scattering to confirm their effect on the vesicles size and weigh-averaged molar mass. Finally we use atomic force microscopy (AFM) imaging and force spectroscopy in solution to quantitatively evaluate the mechanical effect of C_{60} using the Hertz model modified by Chadwick[25] to determine the elastic modulus of supported bilayers.

2. Materials and Methods

2.1 Materials and Liposome Preparation

DMPC, DPPC, DSPC were purchased from Avanti Polar Lipids (Birmingham, Alabaster, USA). NaCl and KCl were purchased from Sigma-Aldrich (St. Louis, MO, USA). Milli-Q water (Millipore, Billerica, MA, USA) with resistance of 18.2 MΩ cm was used throughout all the experiments. Saturated C_{60} solutions were obtained by dissolving C_{60} (ACROS New Jersey, USA) in chloroform (VWR International Ltd., Leicestershire, UK) to a concentration of 0.25 mg/ml.

Liposomes (SUV) Preparation. 0.5 ml of lipid chloroform solution (0.6 mg/mL) was transferred into glass vials and dried gently with nitrogen to form lipid film. The film was hydrated with 1.0 ml of 20 mM NaCl solution, heated to 70 ^{o}C and sonicated with a probe for 3 min. After sonication, the liposome solution was centrifuged at 1300 rpm for 30 min. to remove multillamelar vesicles; the supernatant was used for the subsequent measurements.

Liposomes (SUV) containing C_{60}, mixed film method. C_{60}-liposomes were also produced by hydration of a mixed film composed of C_{60} and phosphatidylcholine (PC) lipids. In brief, 10 μL of 0.25 mg/ml C_{60} solution in chloroform was added to the 0.6 mg/ml lipid chloroform solution, stirred for 5 min to form a mixed lipid-C_{60} solution that was subsequently dried with nitrogen. The mixed film was hydrated in 20 mM NaCl solution, followed by a step of sonication and centrifugation as above.

2.2 Atomic Force Microscopy (AFM)

All images were recorded with a commercial MFP-3D AFM (Asylum Research, Santa Barbara, CA). Imaging was carried out with Olympus TR800 silicon nitride microcantilevers (nominal spring constant k_n = 0.57 N m^{-1}, Olympus, Tokyo, Japan) in amplitude-modulation mode (AM-AFM) at 24.5 °C temperature. The spring constant of the each cantilever was calibrated using the thermal noise method[27]. Before imaging, the system was left for 1 h to reach thermal equilibrium. For each image, height, amplitude, and phase information were acquired simultaneously.

Extension curves (force *vs.* distance curves) were acquired on different areas of the lipid surface. Typically more than 100 measurements were averaged for determining the mechanical properties presented. Extension and retraction velocity was fixed to 200 nm/s for all measurements. For comparison, extension curves where also taken on mica before and after curves acquisition on lipid samples. To avoid systematic errors, each set of measurements carried out in a specific buffer condition was made in a random order.

2.3 Laser Light Scattering (LLS)

A commercial spectrometer from Brookhaven Instruments (BI-200SM Goniometer, Holtsville, NY) was used to perform both static light scattering (SLS) and dynamic light scattering (DLS) over a scattering angular range of 20-120°. A vertically polarized, 100 mW solid-state laser (GXC-III, CNI, Changchun, China) operating at 532 nm was used as the light source, and a BI-TurboCo Digital Correlator (Brookhaven Instruments Corporation) was used to collect and process data.

In SLS, the angular dependence of the excess absolute time-averaged scattered intensity, known as the Rayleigh ratio $R_{vv}(\theta)$, was measured. For a very dilute solution, the weight-averaged molar mass (M_w) and the root mean-square radius of gyration (R_g) were obtained on the basis of

$$HC / R_{vv}(\theta) = (1/M_w)\left[1 + (1/3)R_g^2 q^2\right] + 2A_2 C \qquad (1)$$

where $H = 4\pi^2 n^2 (\mathrm{d}n/\mathrm{d}c)^2/(N_A\lambda^4)$ and $q = 4\pi n/\lambda \sin(\theta/2)$ with N_A, n, dn/dc, and λ being the Avogadro's number, solvent refractive index, specific refractive index increment, and wavelength of light in vacuum respectively.

In DLS, the intensity–intensity time correlation function $G^{(2)}(\tau)$ in the self-beating mode was measured as

$$G^{(2)}(\tau) = A\left[1 + \beta\left|g^{(1)}(\tau)\right|^2\right] \qquad (2)$$

where A is the measured base line, β is a coherence factor, τ is the delay time, and $g^{(1)}(\tau)$ is the normalized first-order electric field time correlation function. $g^{(1)}(\tau)$ is related to the line width distribution $G(\Gamma)$ as

$$g^{(1)}(\tau) = \int_0^\infty G(\Gamma) e^{-\Gamma\tau} d\Gamma \qquad (3)$$

By using a Laplace inversion program, CONTIN, the normalized distribution function of the characteristic line width $G(\Gamma)$ was obtained. The average line width, $\bar{\Gamma}$, was calculated according to $\bar{\Gamma} = \int \Gamma G(\Gamma) d\Gamma$. $\bar{\Gamma}$ is a function of both C and q, which can be expressed as

$$\bar{\Gamma}/q^2 = D(1 + k_d C)\left[1 + f\left(R_g q\right)^2\right] \qquad (4)$$

with D, k_d, f being the translational diffusive coefficient, diffusion second virial coefficient, and a dimensionless constant, respectively. D can be further used to obtain the hydrodynamic radius R_h by using the Stokes-Einstein equation:

$$D = k_B T / 6\pi\eta R_h \quad (5)$$

where k_B, T, η are the Boltzmann constant, absolute temperature and viscosity of the solvent respectively.

For LLS measurements, the aqueous solutions were filtered through 0.20 µm filters (Sartorius Stedim Biotech, Goettingen, Germany).

2.4 Attenuated total reflection (ATR) - Fourier transformed infrared (FTIR) spectroscopy

20 µL of SUVs or SUV/C_{60} solution was deposited on the ATR crystal of the SmartiTR attachment of a Nicolet iS10 (Thermo Scientific) system. FT-IR absorbance spectra were obtained at room temperature with 50 scans averaged for each spectrum. The initial weight ratio of lipid/C_{60} was 120:1.

3. Results and discussion

Incorporation of C_{60} into gel-phase (DPPC) and fluid-phase (DMPC) liposomes, LLS study of size and liposome molar mass

Liposomes of gel and fluid lipids containing C_{60} in the bilayer hydrophobic core were produced by the mixed film method described in the Materials and Methods section, with a C_{60}: lipid weight ratio of 1:120 which is equivalent to ~ 1:120 molar ratio (the molecular weight M_w of PC lipids and C_{60} is very similar, M_w (DPPC) = 734 g/mol and M_w (C_{60}) = 721 g/mol). In dilute solutions, DLS measures time-dependent fluctuations in the scattered light signal using a fast photon counter and can be used to determine the hydrodynamic radius of macromolecules or particles. The radius of gyration and the weight-averaged molar mass of macromolecules or particles can be obtained by fitting the Rayleigh ratio measured in SLS. LLS measurements were performed to characterise the size and molar mass of fluid and gel phase liposomes with or without C_{60} in the bilayer core.

Figure 1A shows the size distribution of DPPC liposomes measured by LLS with or without C_{60} in 20 mM NaCl solution. Only a mono-diffusive mode is observed at all the studied angles and this mode shows no angular dependence. The $R_{h,app}$ (apparent hydrodynamic radius) of liposomes with or without C_{60} after extrapolating to zero angle are 88 and 92 nm, respectively, which is indistinguishable considering the experimental error. The polydispersity of the DPPC/C_{60} liposomes is larger than that of DPPC liposomes. **Figure 1B** compares the angular dependence of the inversed excess scattering intensity in a SLS experiment (denoted as $I_t/(I_s\text{-}I_0)$, with I_t, I_s, and I_0 being the scattered intensity from toluene, liposome solution and the solvent, respectively) of DPPC and DPPC/C_{60} systems. Since the inverted intensity is proportional to $HC/R_{vv}(\theta)$, the inverted intensity after extrapolating to zero angle is proportional to $1/M_{w,app}$, where $M_{w,app}$ is the apparent weigh-averaged molar mass of the studied system. The C_{60}/liposome system has a smaller inverted intensity than that of the lipid-only system which indicates a higher molar mass.

The results of SLS and DLS confirm the incorporation of C_{60} in the SUV by the increase of molar mass (as expected) but small or negligible changes in the size of SUVs, as measured by LLS. Similar results were obtained for fluid lipid DMPC vesicles, *i.e.* successful incorporation with negligible size changes but increased molar mass, as shown in Fig 1 C and 1D. These results confirm the results of the simulations predicting incorporation of C_{60} in the bilayer core[21]. Since in our experiments the C_{60}:lipid molecular ratio is small (~1:120) it can be expected that the presence of C_{60} would not significantly alter the liposome size, since for each 100 nm^2 of bilayer area there should only be ~ 3 C_{60} molecules, in average. To investigate effect on individual lipid molecules, we perform FTIR experiments.

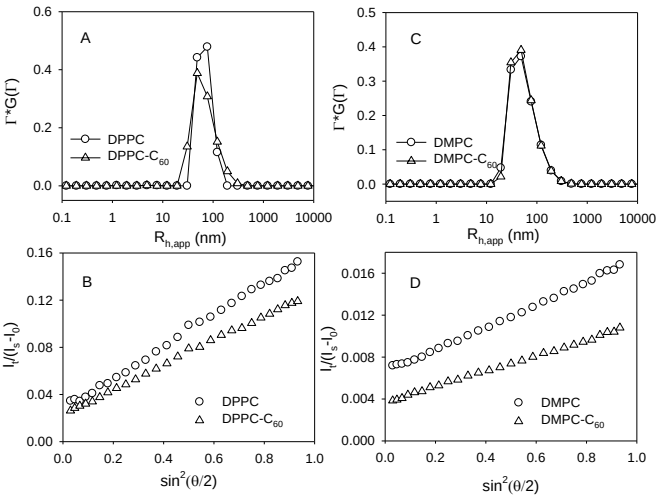

Figure 1. Size distribution at 90° (A&C) and SLS result (B&D) of lipid and lipid/C_{60} systems in 20 mM NaCl solution indicating an increase of the molecular weight of the C_{60} containing liposomes.

Interaction of C_{60} with lipid molecules using FTIR

The interaction between C_{60} and lipid molecules in lipid bilayers was investigated by FTIR using a fluid lipid (DMPC) and a gel phase lipid (DPPC). Additionally to further investigate the effect of the length of the carbon chain in gel lipids we studied DSPC bilayers. Methylene (CH_2X_2) has 9 different vibrational modes, six of which involve only the CH_2 portion: symmetric and anti-symmetric stretching, scissoring, rocking, wagging and twisting[28]. Most of the methylene groups reside in the tail of the lipids and as such, these modes are sensitive to the conformational order of the bilayers. The stretching of CH_2 bonds are sensitive to the changes in the ratio of trans/gauche conformations, an increase in wavenumber is associated with more gauche bonds and therefore lower bilayer order[29]. **Figure 2** shows the asymmetric $\nu_{as}(CH_2)$ (2920 cm^{-1}) stretching band and symmetric $\nu_s CH_2$ (2850 cm^{-1}) of the lipid carbon backbone of different length of carbon tails with or without C_{60}. DPPC and DSPC are both in gel phase at ambient temperature, when C_{60} is present in the bilayer, the CH_2 asymmetric stretching frequency shifts by approximately 1.5 cm^{-1} to the left. In the case of the DPPC and DSPC symmetric stretching frequency, the bonds shift ~2 cm^{-1} and 0.5 cm^{-1} respectively to the lower region with the incorporation of C_{60}, which indicates a reduction in the number of *gauche* bonds. 50 scans were averaged for each spectrum. The wavelength precision is better than 0.01 cm^{-1} at 2000 cm^{-1}, and the spectral resolution is better than 0.4 cm^{-1}. Although the shifts are small, the deviation is larger than 0.4 cm^{-1} and the signal to noise ratio is around 4 for a 1.5 cm^{-1} shift. These results indicate that the presence of C_{60} modifies not only the intra-chain configuration but also the inter-chain orientation of DPPC and DSPC hydrocarbon tail.

To investigate the effect of C_{60} in a lipid in fluid phase we conducted experiments with DMPC. DMPC has a shorter carbon tail and there is no obvious frequency shift for either asymmetric or symmetric CH_2 vibration. This indicates that C_{60} did not affect the lateral packing or chain conformation in DMPC. We note that for DMPC in liquid state the hydrophobic tail has a strong thermal fluctuation leading to a lower-signal to the noise ratio in Fig. 2A.

The combined results of light-scattering and FTIR confirm incorporation in the bilayer core, by an increase of the molecular mass of the liposomes and changes in the inter- and intra-chain orientation of the lipid chains. Furthermore our results indicate that C_{60} molecules do not aggregate inside the vesicles. C_{60} size is about 2/3 of the lipid tail, if they aggregated, the liposome, which is controlled by kinetics, would be probably become unstable and break, which is not observed in the light scattering experiments.

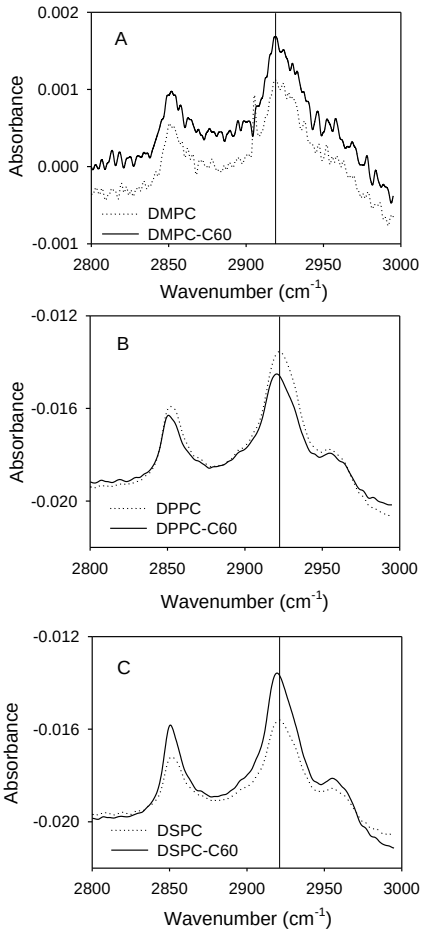

Figure 2. FTIR spectrum of DMPC (A), DPPC (B), and DSPC (C) in the presence/absence of C_{60} inside the bilayer core.

AFM imaging in solution of supported lipid bilayers and unruptured liposomes

Figure 3 shows AM-AFM images recorded in NaCl aqueous solution at room temperature of gel phase DSPC (Fig. 3 A&B), fluid phase DMPC (Fig. 3 C&D), gel phase DPPC (Fig. 3 E&F) and planar bilayers formed after deposition of vesicles on mica. No annealing over the phase transition of the lipids was performed so that information about the vesicle could be inferred. DMPC, DPPC and DSPC share the same PC head-group but have a different length of the hydrocarbon tail (14, 16 and 18 respectively). Left hand-side panels (Fig. 3 A, C&E) show pure lipid bilayers and right hand side panels (Fig. 3 B, D&F) show C_{60}/lipid bilayers. The bilayer height is not appreciably altered by the presence of C_{60} in their interior. The values are (averaging 10 images): 5.44 ± 0.03 nm for DMPC, 5.40 ± 0.14 nm for DMPC/C_{60}; 5.91 ± 0.46 nm for DPPC, 5.72 ± 0.30 nm for DPPC/C_{60}; 5.99 ± 0.28 nm for DSPC, and 6.04 ± 0.21nm for DSPC/C_{60}. The values fit those previously reported in AFM experiments[30]. As expected, increasing the number of methylene of each hydrocarbon tail leads a higher height[31].

Fig. 3 (E&F) show that some liposomes of DPPC do not rupture to form planar bilayers. These un-ruptured DPPC liposomes-like structures would be kinetically trapped structures due to their membrane curvature. These liposome-like structures are not round; they are deformed and present a uniform flatter outer area of around 12 nm in height and a higher central region which height can vary from 16 nm to 30 nm. The height of the outer area suggests that it is 2 bilayers thick and the central region should correspond to a curved structure encapsulating saline solution inside, as proposed in Fig. 3G. The bending point should depend on the curvature of the DPPC lipid membrane; and a larger vesicle produces a higher central region. Based on these data, we propose a scheme for the formation of these structures (Fig. 3G) that could be either due to a liposome attaching directly on mica (left) or a half-ruptured liposome fused on a planar bilayer (right)..

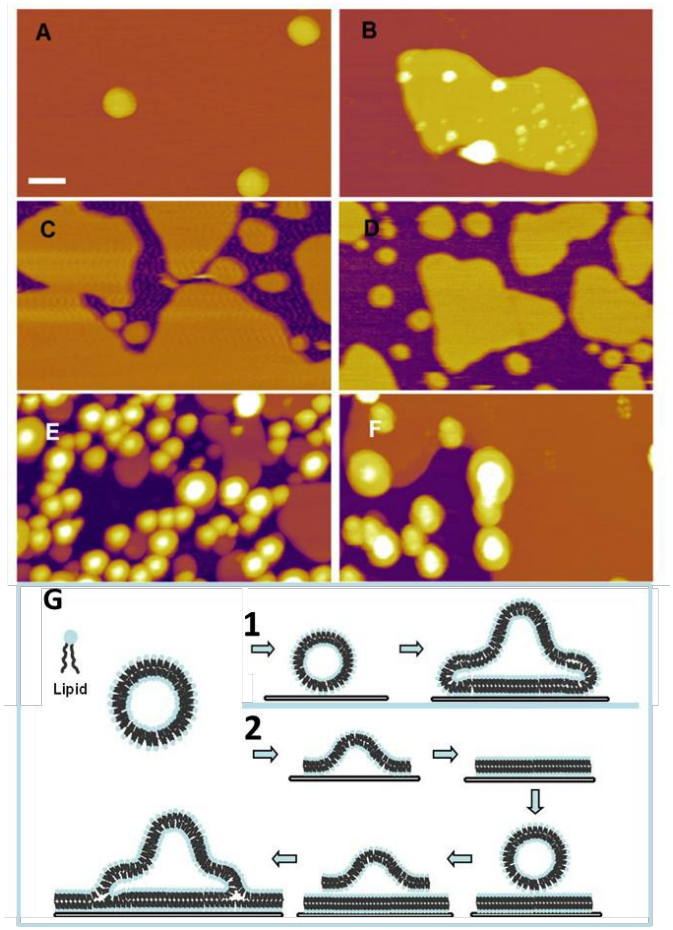

Figure 3. AM-AFM images of lipid bilayers on mica surfaces in 20 mM NaCl solution. (A) DSPC without C_{60}, (B) DSPC with C_{60}, (C) DMPC without C_{60}, (D) DMPC with C_{60}, (E) DPPC without C_{60}, (F) DPPC with C_{60} and (G) Scheme of two hypotheses (1 & 2) of formation of the adsorbed liposome curved structures in 20 mM NaCl solution. Scale bar, 200 nm for all the AFM images.

Force spectroscopy: Effect of C_{60} on modulus of elasticity of planar bilayers

The Young's modulus or modulus of elasticity is an intensive property that characterises a material, independently of its geometry. It is defined as the ratio of the stress to the strain (ratio of deformation over initial length) on one axis in the range of stress in which Hooke's law holds (*i.e.* in the elastic range). AFM indentation allows the determination of the normal Young's modulus of planar bilayers in a direct way, although the examples remain scarce in the literature. One of the main difficulties is that in order to obtain results that are independent of the stiffness of the substrate only a very small part of the indentation curve (1-2 nm) can be used for the fittings, leading to higher experimental errors due to the signal-to noise ratio. Scheuring *et al.*[32] used the Hertz model to calculate the Young's modulus of DPPC in gel (28.1 MPa) and liquid (19.3 MPa) phases, using 20% of the indentation curve. In a previous work we estimated the Young's normal bulk modulus of native purple membranes and its dependence on pH and ionic strength[25] by fitting the force curves with a theory recently developed by Chadwick[33]. This theory is an extension of the Hertz model that assumes a sphere indenting a thin film located on a substrate composed of harder material. In this work we showed that the Young's modulus calculated from the Sneddon's modification of the Hertzian theory systematically shows values 35% higher than the Chadwick model. Here we will use the Chadwick model to calculate the Young's modulus of DPPC and, for the first time, of DMPC and DSPC at 24.5 C, and the influence of C_{60} on their bilayer stiffness. **Figure 4** displays typical force *vs.* indentation curves as the AFM tip moves towards the sample (approach curves) for all the planar lipid bilayers and their corresponding C_{60}/bilayers.

For DMPC no significant change of the slope of the curve during indentation is detected. This seems to indicate that the fluidity of the membrane allows for diffusion of the C_{60} embedded in the fluid bilayer hydrophobic core as the tip deforms it. However there is a clear change of slope for gel-phase lipid membranes that contain C_{60}. Both in DPPC and DSPC force curves show that the resistance of the membrane to the penetrating tip in the presence of C_{60} is higher than that of the pure lipid. We propose that the presence of hydrophobic C_{60} in the bilayer core might change the orientation of the hydrocarbon tails, increasing the cohesion of the hydrophobic part of the membrane and the van der Waals attraction force. Following this interpretation, for DSPC, the increase of stiffness is more evident since DSPC has a longer tail which could provide larger hydrophobic region for C_{60} to interact with. This interpretation is in agreement with the FTIR experiments described above; FTIR indicates that the presence of C_{60} modifies not only intra-chain configuration but also the inter-chain orientation of DPPC and DSPC hydrocarbon tails.

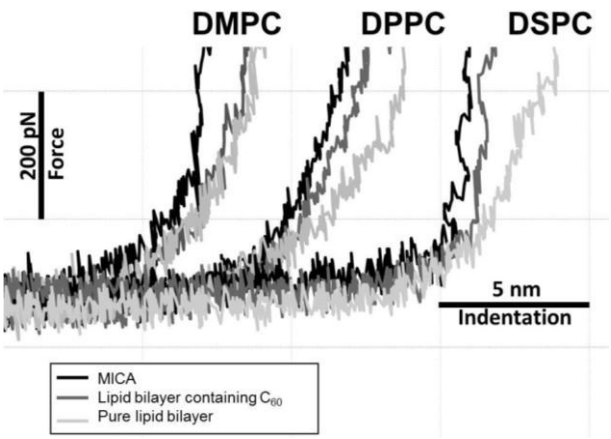

Figure 4. Force vs. indentation curves for pure DMPC, DPPC and DSPC lipid membranes (light grey) and the corresponding C_{60}/lipid systems for each lipid (dark grey), mica is given as reference (black).

To quantify these differences, we calculate the Young's modulus E using the Chadwick model in the elastic part of the indentation curves[33]:

$$F = \frac{2\pi ER}{3h}\delta^2 \qquad (6)$$

where F, R, h, σ are the force, the radius of spherical tip, the thickness of the lipid bilayer and the indentation, respectively. The membrane is considered incompressible (Poisson's ratio ν of 0.5). The results obtained for E using this theory for each lipid bilayer are: 33 ± 13 MPa for DMPC, 34 ± 14 MPa for DMPC/C_{60}; 42 ± 16 MPa for DPPC 69 ± 29 MPa for DPPC/C_{60}; and 51 ± 16 MPa for DSPC, 100 ± 18 MPa for DSPC/C_{60}. These results are plotted in **Figure 5**. Figure 5 clearly demonstrates that the stiffening of the bilayer due to C_{60} in the hydrophobic core increases with the length of the tail of the phospholipid molecule. The values for E quantitatively agree with previously reported values, including Scheuring *et al.* AFM report for DPPC[26, 32]. An additional result of these experiments is a comparison of E values obtained with AFM for bilayers of PC lipids with different number of carbons, which has not been reported before, to the best of our knowledge.

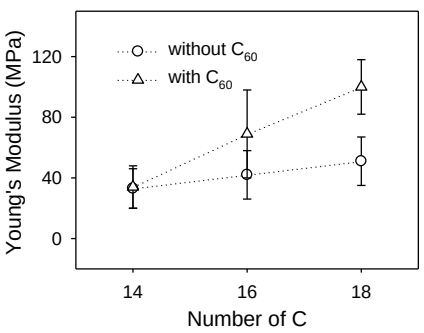

Figure 5. Young's modulus of elasticity *vs.* number of carbons of the phospholipid molecule (14 for DMPC fluid, 16 for DPPC gel and 18 for DSPC gel) of lipid bilayers with and without C_{60} embedded in the bilayer hydrophobic core at 24.5 C.

Bilayer rupture force in DPPC/C_{60} adsorbed liposome structures.

As described above and shown in Fig. 3 (E and F), DPPC samples present unruptured liposomes that form curved structures on the sample. We performed indentation experiments on these un-ruptured structures. During the indentation experiments, in 1/3 of the force *vs*. distance curves on DPPC/C_{60} adsorbed liposome structures we observed a sudden jump-in in the force *vs.* z-displacement curves that corresponds to the rupture of the bilayer[36]. **Fig. 6** shows 6 examples where indentation of adsorbed liposome structures leads to a rupture of the bilayer; the curves present 3 regions labelled as I-III in the figure. Region I is the non-contact region where the tip is far away from the liposome. Region II represents the elastic deformation of the liposome under tip compression. Region III corresponds to the deflection of the lever after penetrating the vesicle. Statistically (by averaging over 60 curves, as shown in the histogram in Fig. 7) the rupture force is 2.7 $\pm$ 1.1 nN which is a considerable reduction from the 20 nN measured by Garcia–Manyes *et al.* for DPPC planar bilayers[36]. However the rupture force strongly depends on the lipid bilayer configuration (planar *vs.* adsorbed liposome) and would also be affected by the material of the tip, differences in temperature and the solution conditions, all these factors can contribute to the order of magnitude difference. However we were only able to measure bilayer rupture events in the presence of $C_{60,}$ not in pure DPPC adsorbed liposomes with the cantilever and forces used for this study. This seems to indicate an alteration of lipid mobility in the presence of C_{60} that would make it easier to penetrate the bilayer in the presence of C_{60} which is in agreement with the FTIR spectroscopy data summarised in Fig. 2.

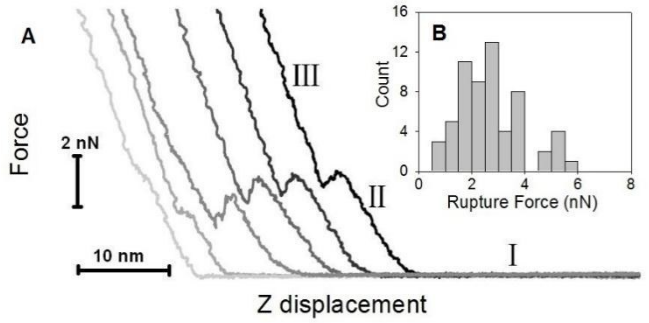

Figure 6. (A) Rupture force for 6 different selected absorbed DPPC/C_{60} SUV vesicles. The presence of C_{60} decreases the mechanical stability of the membrane. The inset (B) shows the histogram of rupture force for total 60 different absorbed DPPC/C_{60} SUV vesicles.

4. Conclusions

The combination of FTIR, AFM and LLS demonstrate the incorporation of C_{60} inside the hydrophobic lipid bilayer core using the mixed film method. FTIR experiments indicate that the presence of C_{60} modifies not only intra-chain configuration but also the inter-chain orientation of DPPC and DSPC hydrocarbon tails, as we summarise in the schematic of **Fig. 7**. AFM imaging confirms previous theoretical studies that predicted no bilayer rupture, micellation or persistent pore formation[21]. Our experiments also indicate that C_{60} molecules are not aggregated inside the bilayer. Our indentation studies show that the modulus of elasticity of supported bilayers increases in the gel phase bilayers after incorporation of C_{60}, but not in fluid phase lipids. The increase is higher for a longer hydrocarbon chain: 1.6 times for DPPC and twice for DSPC. The bilayer rupture force of adsorbed liposomes decreased 10 times with respect to pure DPPC bilayers. Our combined results of AFM indentation and FTIR indicate that C_{60} causes an alteration of gel phase lipid mobility. These results confirm simulation studies that predicted a 40% decrease of the diffusion coefficient of lipids and a significant decrease in mechanical resistance of the membrane[21].

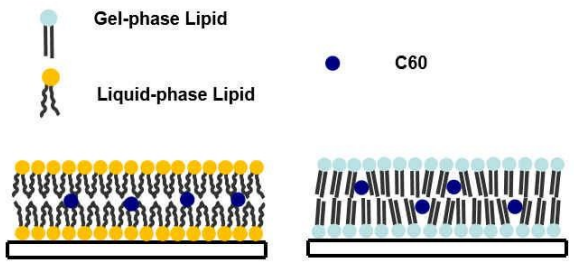

Figure 7. Schematic of the effect of C_{60} on gel and liquid-phase PC bilayers. Well-dispersed C_{60} affects intra- and inter-chain orientation of carbon chains in gel DPPC and DSPC but does not alter DMPC liquid-phase bilayers. In gel phase bilayers, the presence of C_{60} affects the lipid mobility, increases the modulus of elasticity, and decreases the bilayer rupture force. The presence of C_{60} does not affect fluid bilayers' elastic modulus.

Acknowledgements

J.Z. acknowledges financial support by the Chinese Scholarship Council and S. C. from a STFC RCaH grant and support from the Oxford Martin School. Discussions with Sonia Trigueros are acknowledged.

Notes and references

[a] Oxford Martin Programme on Nanotechnology, Department of Physics, University of Oxford, Parks Road, Oxford, UK, OX1 3PU

[b] Beijing National Laboratory for Molecular Sciences and the Key Laboratory of Polymer Chemistry and Physics of Ministry of Education, College of Chemistry and Molecular Engineering, Peking University, Beijing, China, 100871

† Corresponding author: Sonia Contera, Tel: +44 (0) 1865 272269, Fax: +44 (0) 1865 272400, Email: s.antoranzcontera1@physics.ox.ac.uk

1. C. Z. Li, H. L. Yip and A. K. Y. Jen, *J Mater Chem*, 2012, 22, 4161-4177.
2. T. Da Ros and M. Prato, *Chem Commun*, 1999, 663-669.
3. R. Bakry, R. M. Vallant, M. Najam-Ul-Haq, M. Rainer, Z. Szabo, C. W. Huck and G. K. Bonn, *Int J Nanomed*, 2007, 2, 639-649.
4. J. L. R. Ferreira, D. M. Barros, L. A. Geracitano, G. Fillmann, C. E. Fossa, E. A. de Almeida, M. D. Prado, B. R. A. Neves, M. V. B. Pinheiro and J. M. Monserrat, *Environ Toxicol Chem*, 2012, 31, 961-967.
5. C. M. Sayes, J. D. Fortner, W. Guo, D. Lyon, A. M. Boyd, K. D. Ausman, Y. J. Tao, B. Sitharaman, L. J. Wilson, J. B. Hughes, J. L. West and V. L. Colvin, *Nano Lett*, 2004, 4, 1881-1887.
6. R. Sijbesma, G. Srdanov, F. Wudl, J. A. Castoro, C. Wilkins, S. H. Friedman, D. L. Decamp and G. L. Kenyon, *J Am Chem Soc*, 1993, 115, 6510-6512.
7. A. Kumar and S. K. Menon, *Eur J Med Chem*, 2009, 44, 2178-2183.
8. K. Braun, L. Dunsch, R. Pipkorn, M. Bock, T. Baeuerle, S. F. Yang, W. Waldeck and M. Wiessler, *Int J Med Sci*, 2010, 7, 136-146.

9. J. Q. Fan, G. Fang, F. Zeng, X. D. Wang and S. Z. Wu, *Small*, 2013, 9, 613-621.
10. X. Q. Cai, H. Q. Jia, Z. B. Liu, B. Hou, C. Luo, Z. H. Feng, W. X. Li and J. K. Liu, *J Neurosci Res*, 2008, 86, 3622-3634.
11. S. A. Andujar, F. Lugli, S. Hofinger, R. D. Enriz and F. Zerbetto, *Phys Chem Chem Phys*, 2012, 14, 8599-8607.
12. A. S. Basso, D. Frenkel, F. J. Quintana, F. A. Costa-Pinto, S. Petrovic-Stojkovic, L. Puckett, A. Monsonego, A. Bar-Shir, Y. Engel, M. Gozin and H. L. Weiner, *J Clin Invest*, 2008, 118, 1532-1543.
13. S. Kato, R. Kikuchi, H. Aoshima, Y. Saitoh and N. Miwa, *J Photoch Photobio B*, 2010, 98, 144-151.
14. A. Ikeda, M. Mori, K. Kiguchi, K. Yasuhara, J. Kikuchi, K. Nobusawa, M. Akiyama, M. Hashizume, T. Ogawa and T. Takeya, *Chem-Asian J*, 2012, 7, 605-613.
15. A. Ikeda, K. Kiguchi, T. Shigematsu, K. Nobusawa, J. Kikuchi and M. Akiyama, *Chem Commun*, 2011, 47, 12095-12097.
16. V. P. Torchilin, *Nat Rev Drug Discov*, 2005, 4, 145-160.
17. S. Q. Zhang, Y. G. Mu, J. Z. H. Zhang and W. X. Xu, *Plos One*, 2013, 8.
18. J. Barnoud, G. Rossi and L. Monticelli, *Physical Review Letters*, 2014, 112.
19. G. Rossi, J. Barnoud and L. Monticelli, *Phys Scripta*, 2013, 87.
20. J. S. Sun, L. Zhang, J. L. Wang, Q. Feng, D. B. Liu, Q. F. Yin, D. Y. Xu, Y. J. Wei, B. Q. Ding, X. H. Shi and X. Y. Jiang, *Adv Mater*, 2015, 27, 1402-+.
21. J. Wong-Ekkabut, S. Baoukina, W. Triampo, I. M. Tang, D. P. Tieleman and L. Monticelli, *Nat Nanotechnol*, 2008, 3, 363-368.
22. S. Garg, A. A. Thomas and M. A. Borden, *Biomaterials*, 2013, 34, 6862-6870.
23. T. Saxer, A. Zumbuehl and B. Muller, *Cardiovasc Res*, 2013, 99, 328-333.
24. M. N. Holme, I. A. Fedotenko, D. Abegg, J. Althaus, L. Babel, F. Favarger, R. Reiter, R. Tanasescu, P. L. Zaffalon, A. Ziegler, B. Muller, T. Saxer and A. Zumbuehl, *Nat Nanotechnol*, 2012, 7, 536-543.
25. K. Voitchovsky, S. A. Contera, M. Kamihira, A. Watts and J. F. Ryan, *Biophys J*, 2006, 90, 2075-2085.
26. N. Delorme and A. Fery, *Phys Rev E*, 2006, 74.
27. S. Cook, T. E. Schaffer, K. M. Chynoweth, M. Wigton, R. W. Simmonds and K. M. Lang, *Nanotechnology*, 2006, 17, 2135-2145.
28. R. Lu, W. Gan, B. H. Wu, Z. Zhang, Y. Guo and H. F. Wang, *J Phys Chem B*, 2005, 109, 14118-14129.
29. H. H. Mantsch and R. N. Mcelhaney, *Chem Phys Lipids*, 1991, 57, 213-226.
30. H. A. Rinia, R. A. Kik, R. A. Demel, M. M. E. Snel, J. A. Killian, J. P. J. M. van der Eerden and B. de Kruijff, *Biochemistry-Us*, 2000, 39, 5852-5858.
31. N. Kucerka, M. P. Nieh and J. Katsaras, *Bba-Biomembranes*, 2011, 1808, 2761-2771.
32. L. Picas, F. Rico and S. Scheuring, *Biophys J*, 2012, 102, L1-L3.
33. R. S. Chadwick, *SIAM J. Appl. Math.*, 2002, **62**, 1520–1530.
34. L. D. Landau, E. M. Lifshits, A. d. M. Kosevich and L. P. Pitaevskiĭ, *Theory of elasticity*, Pergamon Press, Oxford Oxfordshire ; New York, 3rd English edn., 1986.
35. D. H. Boal, *Mechanics of the cell*, Cambridge University Press, Cambridge, UK ; New York, 2002.
36. S. Garcia-Manyes and F. Sanz, *Bba-Biomembranes*, 2010, 1798, 741-749.